Structural characterization and porosity analysis in self Alumina-silica thin films

T.H.Y. Tran[a]
H. Schut[b]
W.G. Haije[a,c]
J. Schoonman[a]

[a]Delft University of Technology, Faculty of Applied Sciences, Department ChemE, P.O. Box 5045, 2600 GA Delft, The Netherlands
[b]Delft University of Technology, Faculty of Applied Sciences, Department R3, P.O. Box 5045, 2600 GA Delft, The Netherlands
[c]Energy Research Centre of the Netherlands, Hydrogen and Clean Fossil Fuels, P.O. Box 1, 1755 ZG Petten, The Netherlands

Published in Elsevier 520 (2011) 30-34

ECN-W--11-043 OCTOBER 2011

Thin Solid Films 520 (2011) 30–34

Contents lists available at ScienceDirect

Thin Solid Films

journal homepage: www.elsevier.com/locate/tsf

Structural characterization and porosity analysis in self-supported porous alumina-silica thin films

T.H.Y. Tran [a], H. Schut [b], W.G. Haije [a,c,*], J. Schoonman [a]

[a] Delft University of Technology, Faculty of Applied Sciences, Department ChemE, Delft, The Netherlands
[b] Delft University of Technology, Faculty of Applied Sciences, Department R3, Delft, The Netherlands
[c] Energy Research Center of the Netherlands, Hydrogen and Clean Fossil Fuels, Petten, The Netherlands

ARTICLE INFO

Article history:
Received 9 July 2010
Received in revised form 11 June 2011
Accepted 14 June 2011
Available online 21 June 2011

Keywords:
Silica
Alumina
Sol-gel
Positron Doppler broadening analysis
Nitrogen
Physisorption
X-ray diffraction
Fourier transform infrared spectroscopy

ABSTRACT

In this study, alumina, silica and alumina-silica binary (36% mol silica) thin films are synthesized using the sol-gel technique. These form the basis for future gas separation membranes. The characterization of the synthesized oxides was performed using nitrogen physisorption, X-ray diffraction (XRD), Doppler-broadening measurements on the 511 keV annihilation photon peak, together with 3γ/2γ analysis, and Fourier transform infrared spectroscopy (FTIR) of adsorbed CO. It is found that silica is microporous, γ-alumina is mesoporous, and the binary material shows fingerprints of both the meso- and microporous nature of its constituents as well as of the respective crystal structures. These results open the possibility to also investigate thin supported porous films (a few microns thick), and especially the setting and drying aspects on porous supports for membrane production, using the positron annihilation technique.

1. Introduction

The field of nanoporous inorganic materials (pore sizes between 1 and 100 nm) is experiencing explosive growth in a widening field of important applications, such as catalysis in chemical engineering and fuel production [1], purification and separations [2], and clean energy production and carbon capture [3,4]. Mature synthesis technologies, such as the sol-gel technique, have been developed to produce materials with flexibility and tailor-made porosity and pore size [5]. Sol-gel based thin films and membranes have been extensively studied in previous decades, but still trigger the interest of material scientists active in this field. In particular, the improvement of inorganic porous membranes to operate in hostile chemical environments and under crucial pressure and temperature conditions, as opposed to the limited polymeric membrane operating window, is an issue that many scientific publications [6–8] and review papers [2,9] deal with. Among sol-gel derived membranes developed to date, amorphous microporous silica membranes are the most notable of inorganic membranes with the capability of separating H_2 from mixed gas streams. However, microporous silica materials are not hydrothermally stable, due to the degradation of the silica microstructure in the presence of water vapor or liquid which results in hydrolysis of siloxane bridges (Si–O–Si) both at low [6] and high temperatures [12], and the rupture of the whole membrane layer. Therefore, improving the hydrothermal stability of microporous SiO_2 membranes has received much attention. One of the options for instance is doping the starting silica sol with a metal oxide such as Al_2O_3, TiO_2, ZrO_2, or NiO [10–13]. For example, the alumina-doped silica membrane exhibited separation properties similar to the pure silica membranes and the hydrothermal stability was improved after doping with 3% alumina [10]. Upon exposure to 50 mol% steam/air at 600 °C for 30 h, the alumina-doped silica had 64% reduction in the surface area and a loss of 86% micropore volume, compared to 85% and 94%, respectively, for the pure silica.

The effectiveness of the alumina-silica binary is also the subject of our research. In an attempt to obtain binary alumina-silica membranes with tailor-made porosity features, different mixed Al–Si compositions were prepared by controlling the molar Al/Si ratio range of 0–100 mol% Si. In the present study, the alumina-silica binary with 36 mol% Si is selected, because it starts showing the evident fingerprints of both the meso- and microporous nature of its constituents. More important than the porous properties of the alumina-silica binary system is its homogeneity in the preparation. The porous structure of this composite self-supported film is investigated and compared to those of pure γ-alumina and silica. The quantitative information from the N_2 physisorption technique,

* Corresponding author at: Energy Research Center of the Netherlands, Hydrogen and Clean Fossil Fuels, Petten, The Netherlands. Tel.: +31 224 564790.
E-mail address: haije@ecn.nl (W.G. Haije).

0040-6090/$ – see front matter © 2011 Elsevier B.V. All rights reserved.
doi:10.1016/j.tsf.2011.06.027

the X-ray diffraction (XRD), the positron annihilation Doppler broadening (PADB) technique, and Fourier transform infrared (FTIR) spectroscopy of adsorbed CO are complementary to each other and together help in assessing the micro-structural properties of the alumina-silica self-supported film. The interesting point of the study is to highlight the advantage of positron in PADB technique to probe nanostructure of porous thin films for membrane applications.

2. Experimental details

2.1. Thin film synthesis

All samples were prepared using the sol-gel technique, using either a boehmite sol or a silica sol or a mixture of both. The boehmite sol was synthesized by the colloidal route [8]. Aluminum tri-sec-butoxide (ASB, 99% purity, Sigma-Aldrich) was added to water at 80 °C under vigorously stirring. Two litres of water were used per mol of alkoxide. The solution was kept at 90 °C and, about half to 1 h after addition of the alkoxide, 0.07 mol HNO_3 (Sigma-Aldrich) per mol alkoxide was added to peptize the sol. The sol was kept boiling in an open reactor for about 2 h to evaporate most of the butanol and was subsequently kept at 90 °C during about 16 h under reflux conditions. The final boehmite sol had a transparent light-blue color and the AlOOH concentration was 0.92 M.

The polymeric silica sol was prepared by acid-catalyzed hydrolysis and condensation of tetraethyl-orthosilicate (TEOS, purity 99.9% Sigma-Aldrich) in ethanol (purity>99.9 Merck). Molar ratios of TEOS/water/HNO_3/ethanol were 1.0/6.4/0.085/3.8. The sol was prepared by careful drop-wise addition of water and acid to the TEOS ethanol solution followed by 2 h refluxing at 80 °C under stirring [14].

A small amount of boehmite or silica sol was poured into different Petri dishes. Mixed alumina/silica samples were prepared by mixing a boehmite and polymeric silica sol beforehand in the targeted proportions of Al_2O_3/SiO_2. The sample used for this study contains 36 mol% of SiO_2. After drying for 3–5 days under ambient conditions, the samples were calcined at 600 °C for 3 h with a heating rate of 60 °C/h. In order to have a sufficient mechanical strength, the self-supported thin films with approximately dimensions of 10 mm × 10 mm × 1 mm were prepared for the characterizations.

2.2. Characterization

A conventional pore-size analysis method, i.e., N_2 physisorption was used to assess the total surface area and the pore size distribution. These measurements were carried out in an Autosorb 1-B physisorption set-up (Quantachrome Instruments). The samples were degassed at 150 °C under vacuum ($P<10^{-3}$ Pa) for 16 h. From the change in pressure due to the adsorption (desorption) and known gas volume at 77 K (liquid N_2 normal boiling point), the quantity of adsorbed (desorbed) N_2 can be calculated when the dead volume is calibrated by a non-adsorbing gas like He. The specific surface area can thus be deduced from the N_2 isotherm data in the relative pressure P/P_0 range of 0.05–0.30, using the Brunauer, Emmett, and Teller (BET) equation [15]. For the calculation of the pore size distribution the density functional theory (DFT) [16,17] and the Horvath Kawazoe model (HK) [20] were applied for the mesopores (diameter of 2–50 nm) and micropores (diameter<2 nm), respectively. The total pore volume V_p is calculated from the N_2 volume ($cm^3\,g^{-1}$) adsorbed at the relative pressure of 0.975. According to the Gurvitsch rule, under the assumption that N_2 is adsorbed in liquid form, the total pore volume V_p ($cm^3\,g^{-1}$) is estimated as follows:

$$V_p = V_{ads} \times 1.547 \times 10^{-3} \quad (1)$$

where V_{ads} is the N_2 saturation adsorption volume ($cm^3\,g^{-1}$). The density of N_2 in the pores is assumed to be that of liquid N_2 (i.e., 0.808 g cm^{-3}). The total pore volume V_p is also used to calculate the porosity. The porosity is defined as the ratio of the total pore volume to the total volume of a sample V ($cm^3\,g^{-1}$). The total volume V of the sample is directly related to the density of the sample ρ (g cm^{-3}) as follows:

$$V = V_p + 1/\rho \quad (2)$$

The wide-angle XRD measurements were performed with a Bruker D8 Advance diffractometer using the Cu Kα radiation (λ = 1.54178 Å) of a conventional X-ray source powered at 40 kV and 50 mA. The diffraction patterns were obtained by scanning the samples from 10°–80° (2θ), with a counting time of 5 s per step with a step of 0.02° in a continuous scan mode to identify the metal oxide phases present.

Positron annihilation spectroscopy is based on the fact that positrons, the positive anti-particle of electrons, annihilate with electrons in the subjected material, resulting in two γ rays according to the energy-matter equation $E = mc^2$ which is 511 keV for an electron. Positrons can form positronium (Ps), a hydrogen-like bound state with an electron, when positrons are injected into a pore. Ps gradually dissipates its energy by means of inelastic collisions with the pore wall. Even epithermal Ps ($E>kT$) is not able to re-enter the solid and remains confined to the pore volume. However, connected pores forming clusters allow Ps motion on a larger length-scale. Therefore, both thermal and epithermal Ps can escape from the sample by finding a route through an open pore to the sample surface and Ps emission into the vacuum may be observed. Ps initially forms in two states, para, p-Ps (↑↓ electron-positron spin configuration) and ortho o-Ps (↑↑), whose annihilation characteristics are different. p-Ps annihilates into two photons (2γ), with a lifetime in vacuum of 0.125 ns. o-Ps annihilates into three photons (3γ) by self-annihilation or annihilates with an electron from the pore wall into two photons (2γ) by the so-called "pickoff" annihilation. The probability of the latter depends on the collision frequency with pore walls which can shorten the *o*-Ps lifetime (its initial lifetime in vacuum is 142 ns). The rate of "pickoff" annihilation is related to the size of the pore because of its dependence on the electron density in the annihilation site. It influences the ratio of the 3γ/2γ annihilation peak intensity and can, therefore, be used to derive porosity properties. In this study, the PADB experiments were performed at the Reactor Institute Delft using the Delft variable energy positron beam. All experiments were carried out at room temperature under a vacuum of 10^{-6} Pa. In this setup positrons emitted from a ^{22}Na source are moderated to thermal energies, subsequently accelerated, and then injected into the samples with a kinetic energy E tuned between 100 eV and 25 keV. The annihilation spectrum recorded at each positron implantation energy E is analyzed for two parameters, i.e., the 3γ/2γ annihilation ratio (given by the R parameter) and the Doppler broadening of the annihilation radiation (given by the S parameter). The R parameter is the ratio between the number of 3-γ counts (T) in the low-energy region ($E_\gamma<511$ keV) and the total number of counts (P) in the annihilation spectrum around 511 keV. The S-parameter is defined as the ratio between the number of counts in a chosen, fixed central region, to the number of counts in the entire 511 keV annihilation peak.

The mean implantation depth $\langle z \rangle$ (nm) of the positrons into the sample is given by:

$$\langle z \rangle = \frac{A}{\rho} E^{1.62} \quad (3)$$

where A is a material independent parameter (40 μg cm^{-2} $keV^{-1.62}$), ρ is the density of the sample (g cm^{-3}), and E is the positron implantation energy (keV). For example, in alumina ($\rho \sim 3.9$ g cm^{-3}) positrons with an energy of 25 keV have a mean implantation depth of about 2 μm.

For in-situ FTIR measurements, pellets of the samples were prepared and placed inside an IR cell which allowed in-situ high-temperature treatments, CO dosage, and IR measurements at liquid nitrogen temperature to be made. CO is a weakly basic probe molecule which is particularly suitable to probe the presence of Brønsted acid sites. When interacting with acid hydroxyl groups, the OH · · · CO acid/base adducts lead the perturbations of the vibrational frequencies (or wavenumbers) of OH and CO stretching modes. The positions of the OH and CO vibrational bands and their behaviors (wavenumber shifts) upon CO adsorption can be directly related to the acidic strength of bridging hydroxyl groups of Brønsted acid sites and Lewis acid sites [19–23]. The IR spectra were recorded with a Bruker Equinox 55 spectrometer at 2 cm^{-1} resolution. The spectra are presented in absorbance scale after normalization with respect to the pellet weights.

3. Results and discussion

The porous characteristics for γ-alumina, silica, and the alumina-silica (36 mol% Si) binary obtained by the N_2 adsorption–desorption measurements are summarized in Table 1. As shown in Fig. 1, the pure γ-Al_2O_3 sample has an isotherm of type IV according to the IUPAC classification [24] with N_2 hysteresis loop between the relative pressures P/P_0 of 0.4–0.75, which is characteristic for mesoporous material. A similar isotherm type with a smaller hysteresis loop is also observed for the binary sample. However, the binary sample has a higher volume of N_2 adsorption at low P/P_0<0.4, which reflects an important amount of micropores along with mesopores in the structure. Therefore, it has a higher BET surface area than that of γ-Al_2O_3. The BET surface area of the binary sample is about 380 $m^2\ g^{-1}$, while that of γ-Al_2O_3 is 280 $m^2\ g^{-1}$. The porosities are estimated to be 40% and 48%, respectively. On the other hand, the isotherm observed for the SiO_2 sample is very different in that the absence of a hysteresis loop, which is assigned to a type I [18] and characteristic for microporous material. The SiO_2 sample yields a highest surface area of 480 $m^2\ g^{-1}$ and a porosity of ~34%. No trend about the relationship between the surface area and pore volume can be deduced from these results, but there is concern that sintering effects can occur at the high calcination temperature of 600 °C and may result in a denser structure of SiO_2.

The porosity features of all samples are better understood by analyzing the pore-size distributions. Pure γ-Al_2O_3 is characterized by a broad pore size distribution with a mean pore size of 5.5 nm as shown in Fig. 2. In the binary sample, a bimodal pore size distribution with maxima around 3 nm and 0.5 nm can be seen from the combined results obtained from the DFT model (Fig. 2) and those from the HK model (Fig. 3). The two models do not give the same pore size distribution because the DFT method based on the Kelvin equation (is reliable in the mesopore region) and the HK method is strictly only valid for micropores (<2 nm). The DFT and HK results on the SiO_2 sample, however, both yield a pore size distribution in the small pore range of 0.5–2 nm.

The wide-angle XRD patterns for the γ-alumina, silica, and the alumina-silica binary samples are presented in Fig. 4. The observed peaks corresponding to the gamma phase appear obviously in the XRD pattern of γ-alumina sample. The XRD pattern of silica contains only a broad peak characteristic of amorphous silica, which can be discerned around 24°. The binary sample presents two broad peaks with low intensities, at approximately 47° and 67°, which are close to the position of the strongest peaks in the γ-alumina system. There is also an increase in the background signals at the right angle hinting at the presence of silica. The alumina-silica sample, however, is rather amorphous which hampers a clear-cut identification of other possible phases' presence. Thus, the XRD results need to be substantiated with results obtained from other complementary techniques. The PADB and FTIR will then provide the conclusive information.

Table 1
Structural characteristics for γ-alumina, silica, and the alumina-silica (36% Si) binary samples (*according to the IUPAC classification [24] and all standard deviations were obtained with triplicated measures).

Samples	Isotherm type (*)	BET area ($m^2\ g^{-1}$)	Pore volume V_p ($cm^3\ g^{-1}$)	Porosity (%)	Mean pore diameter D (nm)
Al_2O_3	IV	280 ± 17	0.236 ± 0.03	48 ± 1.44	5.5 ± 0.4
SiO_2	I	480 ± 29	0.230 ± 0.03	35 ± 1.05	2 ± 0.5
Al_2O_3/	IV	380 ± 23	0.229 ± 0.02	40 ± 0.8	0.5 ± 0.1 and 3 ± 0.5

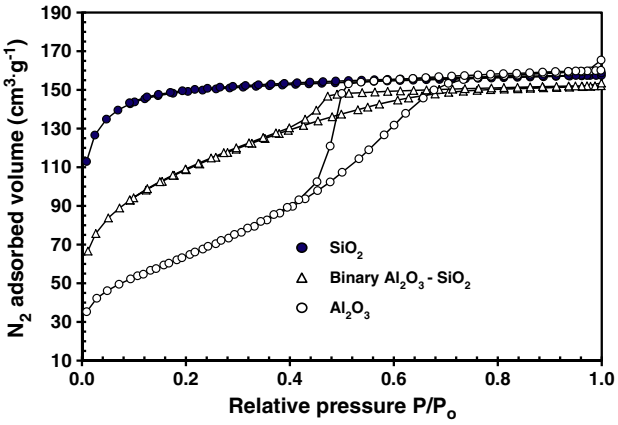

Fig. 1. Nitrogen physisorption isotherms of γ-alumina, silica, and the alumina-silica binary.

The surface and up to two microns in-depth of the as-prepared thin films are investigated by PADB. From the *R*-parameter data a clear distinction can be made between the pure γ-Al_2O_3 and the other two samples. The trend of the curve in the pure γ-Al_2O_3 (Fig. 5) shows that o-Ps annihilation decay via *R* (3γ/2γ annihilation ratio) is observed up to the maximum positron implantation energy. The 3γ decay originates from the o-Ps self-annihilation, which is reflected in the *R*-parameter, i.e., an increase in the 3γ annihilation contributes to the increase of *R*. The binary sample only shows a relevant amount of 3γ decay events up to a depth of approximately 80 nm (see upper axis of Fig. 5). This increase at such low incident positron energies is attributed to the back-scattering of non-thermalized or fast positrons that pick up electrons at the surface and escape back to vacuum as fast Ps (p-Ps and o-Ps). For the pure silica sample the o-Ps signal extends to a somewhat larger depth of about 200 nm. This is attributed to additional back-diffusion of thermalized positrons to the surface followed by the emission of thermal Ps. The Doppler broadening of positron-

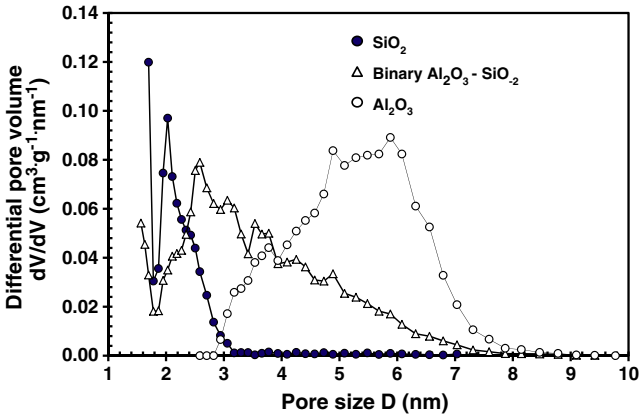

Fig. 2. Mesoporous size distribution obtained by density functional theory (DFT) for γ-alumina, silica, and the alumina-silica binary.

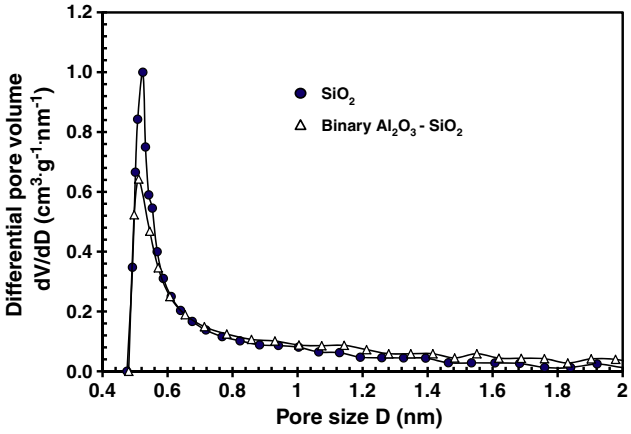

Fig. 3. Microporous size distribution of silica and the alumina-silica binary obtained by the Horvath Kawazoe (HK) model.

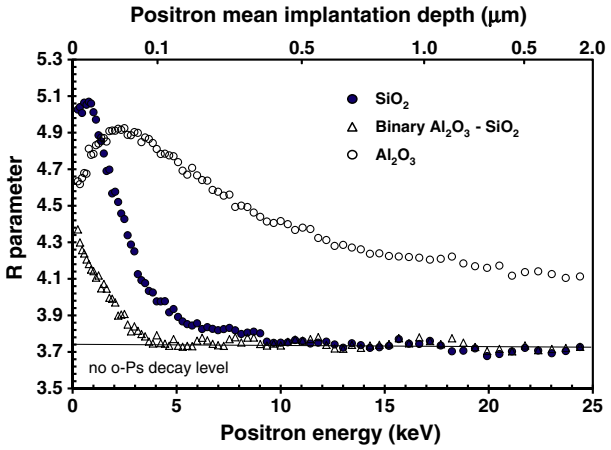

Fig. 5. The *R* parameter as a function of positron implantation energy (bottom *x*-axis) and corresponding mean implantation depth (top *x*-axis).

annihilation measurements are presented by the *S*-parameter versus mean positron implantation energy (mean positron implantation depth, upper axis as shown in Fig. 5).

As for the *R* parameter, with increasing positron implantation energy, the *S* parameter firstly characterizes the surface, then the sub-surface, and finally the bulk up to a depth of about 2 μm. As shown in Fig. 6, no significant difference between pure γ-Al_2O_3 and SiO_2 is observed when going from the surface to the interior of the film. The trends of the *S* parameter indicate positron annihilation in a homogeneous layer. In contrast, the binary sample shows lower *S* values. These lower *S* values can be attributed to the reaction of Ps with Brønsted acid sites of the binary material. Huang et al. [25] reported that the Brønsted acid sites are responsible for the change in the annihilation characteristics of Ps by means of its oxidation with Brønsted protons. This reflects the value of *S* parameter, i.e., the decrease in the value of *S* parameter with increasing Brønsted acid sites. By incorporating the silicon atoms into alumina network, the formation of the bridged hydroxyl groups (Brønsted acid sites) Si–OH–Al can be present [22–26]. Therefore, the lower *S* values are observed, which is also indicative of the homogeneous distribution of silica-like domains in a γ-alumina matrix. A minimum of the *S* parameter is observed at an energy of about 3.5 keV, indicating the presence of a sub-surface region or interface capable of effectively trapping positrons and thus preventing back diffusion of thermal positrons towards the surface. The above mentioned energy is in accordance with the onset of the 3γ decay events depicted in Fig. 5. A possible reason for this asymmetry may be explained by the evaporation mechanism that occurs during the drying of the film. The one face is open to the ambient enabling quick drying by evaporation, and then leads to the denser packing of the particles. On the other hand the side in contact with the Petri dish lacks this quick evaporation pathway. The apparent difference in *R*- and *S*-dependence

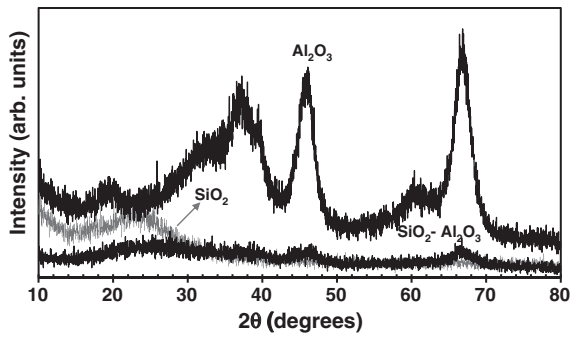

Fig. 4. Wide-angle XRD patterns of γ-alumina, silica, and the alumina-silica binary.

can be accounted for by constructing a branching scheme for the different positron annihilation channels. This has been shown for positron studies of internal pore surfaces in sol-gel-derived silicate films [26]. The general information emerging from the positron data is that in the pure γ-Al_2O_3 pores that are large enough to accommodate Ps formation and the subsequent decay from the o-Ps state are present. The silica sample shows no sign of o-Ps decay via 3γ annihilation, putting an upper limit to the pore size. The high value of *S* (within the experimental uncertainty equal to that of alumina) is attributed to the intrinsic decay of p-Ps. With the settings of the momentum windows for determining the *S* parameter p-Ps decay is expected to yield an *S* of approximately 0.75. The fraction of positrons annihilating from this state accounts for the observed value of *S* and thus hints at the formation of Ps. In the binary sample no o-Ps is observed. In addition, the low *S* value indicates that annihilation channels other than p-Ps decay are involved. This interpretation leads to the conclusion that in the alumina-silica binary sample Ps may preferentially interact with Brønsted protonic sites and annihilates as a free positron.

The presence of Brønsted acid sites in the binary sample, which are absent in pure alumina or silica as already reported in the literature [19–23], is probed by FTIR spectroscopy under CO adsorption. Fig. 7 shows the selected in-situ FTIR spectra 1–6 of CO adsorption on the silica-alumina binary sample at 77 K for different equilibrium pressures. Spectrum 6 represents the highest CO adsorption of the sample. In the CO stretching region one broad and weak band appears initially at 2163 cm^{-1}, then increases its intensity and slightly shifts

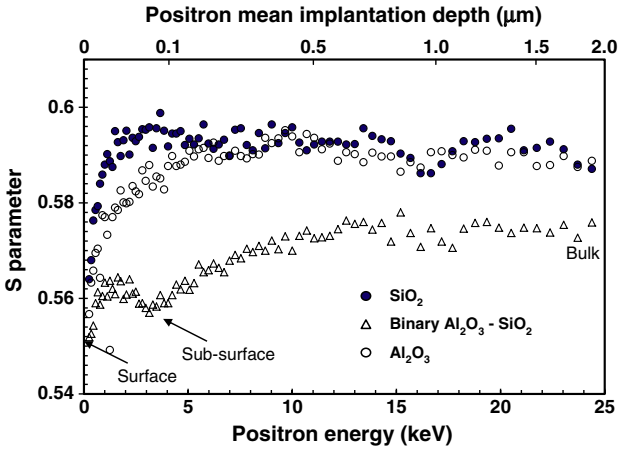

Fig. 6. The *S* parameter as a function of positron implantation energy (bottom *x*-axis) and corresponding mean implantation depth (top *x*-axis).

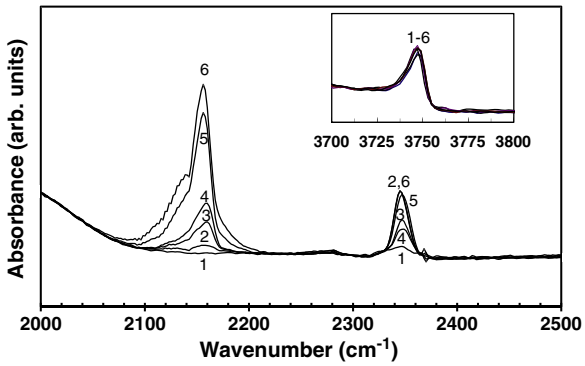

Fig. 7. In-situ FTIR spectra (1–6) of CO adsorption on the alumina-silica binary sample, at 77 K with different equilibrium pressures of 15 Pa, 520 Pa, 540 Pa, 560 Pa, 1400 Pa, and 3500 Pa, respectively.

its position to 2156 cm^{-1} when the CO pressure is increased. This can be assigned to CO adsorbing on the OH of Brønsted acid sites. It should be noted that weak Lewis sites formed by dehydratation of Brønsted acid sites also contributed in this band [23]. The other band growing with less prominent is observed at ~2345 cm^{-1}. According to the literature, this band may be assigned to the formation of CO_2 on Lewis sites [27,28]. In the OH stretching region, sharp bands are present at 3747 cm^{-1}, which are attributed to the silanol (SiOH) groups. Such OH groups with very weak acidity barely interact with a weakly basic CO. The absence of bridging OH stretching bands may be due to the fact that the silanol density is much higher than that of the bridging hydroxyl together with the low signal-to-noise ratio in this region. The FTIR result again points to silica islands in a γ-alumina matrix where the Brønsted sites are on the oxide interface.

4. Conclusions

The investigation of the sol-gel derived porous membranes deposited as self-supported films, has generated a great deal of insight into the meso and microporous nature of their constituents, i.e., silica is microporous, γ-alumina is mesoporous, and the binary shows fingerprints of both the meso- and microporous structure. This is confirmed by all characterisation techniques used. The formation of bridging hydroxyl groups reflected from the positron annihilation and FTIR results reveal that the binary sample consists of more or less homogenous γ-alumina and silica regions with a chemical interaction between these phases. The fact that there are still silica rich regions can be reflected in the inability of other authors to obtain good results on hydrothermally stable membranes upon mixing silica with another metal oxide. Interestingly, the positron annihilation technique, however complex, is very useful to evaluate the structural differences of such porous materials in a wide range of pore sizes and in the presence of specific acidic groups. The use of variable positron implantation energies (in the range of 100 eV–25 keV corresponding to a probe depth up to two microns) has been shown an ideal means for also characterizing porous supported membranes, of which the thickness (the amount of material) is even less than the self-supported films investigated in this work. This technique could be valuable for the assessment of drying mechanisms during membrane preparation, e.g., evaporation rate and capillary suction effects of thin film depositions (a few μm thick) on porous supports in future investigations.

Acknowledgements

The authors wish to thank Stanford University for supporting this work through the Global Climate Energy Project (GCEP) and the sponsors of GCEP. We gratefully acknowledge Prof. F. Kapteijn and his co-workers (Delft University of Technology) for providing access to the Autosorb 1-B, Quantachrome Instrument and FTIR spectroscopy.

References

[1] C.S. Song, Catal. Today 77 (2002) 17.
[2] N.W. Ockwig, T.M. Nenoff, Chem. Rev. 107 (2007) 4078.
[3] P. Benard, R. Chahine, Scr. Mater. 56 (2007) 803.
[4] S.S. Han, J.L. Mendoza-Cortes, W.A. Goddard, Chem. Soc. Rev. 38 (2009) 1460.
[5] C.G. Guizard, A.C. Julbe, A. Ayral, J. Mater. Chem. 9 (1999) 55.
[6] J. Campaniello, C.W.R. Engelen, W.G. Haije, P.P.A.C. Pex, J.F. Vente, Chem. Commun. (2004) 834.
[7] H. Verweij, Y.S. Lin, J.H. Dong, MRS Bull. 31 (2006) 756.
[8] B.C. Bonekamp, A. van Horssen, L.A. Correia, J.F. Vente, W.G. Haije, J. Membr. Sci. 278 (2006) 349.
[9] P. Bernardo, E. Drioli, G. Golemme, Ind. Eng. Chem. Res. 48 (2009) 4638.
[10] G.P. Fotou, Y.S. Lin, S.E. Pratsinis, J. Mater. Sci. 30 (1995) 2803.
[11] Y.F. Gu, S.T. Oyama, J. Membr. Sci. 345 (2009) 267.
[12] K. Yoshida, Y. Hirano, H. Fujii, T. Tsuru, M. Asaeda, J. Chem. Eng. Jpn. 34 (2001) 523.
[13] M. Kanezashi, M. Asaeda, J. Membr. Sci. 271 (2006) 86.
[14] R.M. de Vos, H. Verweij, J. Membr. Sci. 143 (1998) 37.
[15] S. Brunauer, P.H. Emmett, E. Teller, J. Am. Chem. Soc. 60 (1938) 309.
[16] R. Evans, Adv. Phys. 28 (1979) 143.
[17] C. Lastoskie, K.E. Gubbins, N. Quirke, Langmuir 9 (1993) 2693.
[18] G. Horvath, K. Kawazoe, J. Chem. Eng. Jpn. 16 (1983) 470.
[19] W. Daniell, U. Schubert, R. Glockler, A. Meyer, K. Noweck, H. Knozinger, Appl. Catal. A-Gen. 196 (2000) 247.
[20] G. Crepeau, V. Montouillout, A. Vimont, L. Mariey, T. Cseri, F. Mauge, J. Phys. Chem. B 110 (2006) 15172.
[21] M. Trombetta, G. Busca, S. Rossini, V. Piccoli, U. Cornaro, A. Guercio, R. Catani, R.J. Willey, J. Catal. 179 (1998) 581.
[22] V. Gruver, J.J. Fripiat, J. Phys. Chem. 98 (1994) 8549.
[23] J.C. Lavalley, Catal. Today 27 (1996) 377.
[24] K.S.W. Sing, D.H. Everett, R.A.W. Haul, L. Moscou, R.A. Pierotti, J. Rouquerol, T. Siemieniewska, Pure Appl. Chem. 57 (1985) 603.
[25] W.F. Huang, D.C. Huang, P.K. Tseng, Catal. Lett. 26 (1994) 269.
[26] R.E. Galindo, A. van Veen, H. Schut, C.V. Falub, A.R. Balkenende, G. de With, J.T.M. De Hosson, Compos. Sci. Technol. 63 (2003) 1133.
[27] V.M. Rakic, R.V. Hercigonja, V.T. Dondur, Microporous Mesoporous Mater. 27 (1999) 27.
[28] T. Montanari, O. Marie, M. Daturi, G. Busca, Catal. Today 110 (2005) 339.